Sensors and Actuators B 245 (2017) 375–385

Contents lists available at ScienceDirect

Sensors and Actuators B: Chemical

journal homepage: www.elsevier.com/locate/snb

Improving the triethylamine sensing performance based on debye length: A case study on α-Fe_2O_3@NiO(CuO) core-shell nanorods sensor working at near room-temperature

Qi Xu, Zichao Zhang, Xiaopan Song, Shuai Yuan, Zhiwen Qiu, Hongyan Xu, Bingqiang Cao *

Materials Research Center for Energy and Photoelectrochemical Conversion, School of Materials Science and Engineering, University of Jinan, Jinan 250022, Shandong, China

ARTICLE INFO

Article history:
Received 21 September 2016
Received in revised form
29 December 2016
Accepted 22 January 2017
Available online 23 January 2017

Keywords:
Core-shell nanorod
PN heterojunction
Debye length
TEA sensor
Near room-temperature

ABSTRACT

Metal oxide semiconductor (MOS) based gas sensors for triethylamine (TEA) are anticipated with low operating temperature, high response, and robust manufacturing process. TEA sensors with the α-Fe_2O_3@NiO or α-Fe_2O_3@CuO core-shell nanorods (NRs) heterostructure are successfully fabricated and their sensing performance is optimized by controlling the shell thickness based on Debye length. Porous α-Fe_2O_3 NRs are directly prepared on flat Al_2O_3 substrates by convenient hydrothermal process. The p-type shell layer is deposited by pulsed laser deposition (PLD) method, which width is controlled by changing the applied laser pulses. Due to the formation of PN heterojunction, the core-shell NR heterostructures show enhanced performances than pristine α-Fe_2O_3 NRs at near room-temperature, e.g. 40 °C. Moreover, such heterostructural sensor performances also exhibit a strong dependence on the shell thickness. When the p-type shell thickness is close to its Debye length (λ_d), the core-shell sensor of the highest response is realized. The enhanced sensing properties of this core-shell NR heterostructure toward TEA can be explained by the increase of initial resistance (R_a) due to the modulation of depletion layer through optimizing the p-type shell thickness.

1. Introduction

As an important organic amine, triethylamine (TEA) is widely used as preservative, catalyst, synthetic dye, and high energy fuel in industrial production [1]. It can also be released from dead fishes and marine animals, and the concentration increases with the increasing degree of spoilage. TEA is highly toxic and harmful to human body like eye irritation, skin burns, pulmonary edema, and even dead. According to Occupational Safety and Health Administration (OSHA) regulation, its permissible exposure limit is 10 ppm in air [2,3]. Some testing methods like laser-induced fluorescence, gas/liquid/film chromatograph, and electrochemical methods have been adopted to detect TEA gas in ambient environment [4–6]. However, the complex test process, expensive equipment, and rigorous experimental environment restrict their widespread applications. Therefore, it is urgent to develop a low-cost and portable instrument with good selectivity and repeatability to detect TEA gas in daily life or industrial production process.

Recently, MOS gas sensors such as ZnO [3], SnO_2 [7], α-Fe_2O_3 [8,9], V_2O_5 [10], α-MoO_3 [11,12], and TiO_2 [13] attract much attention for real-time environmental monitoring and hazardous gases detecting. α-Fe_2O_3 has exhibited impressive sensing property to acetone [14], toluene [9], trimethylamine [13], formaldehyde [15], and so on. For TEA gas sensor applications, Sun et al. [16] reported mesoporous α-Fe_2O_3 microscale rods to detect TEA and the response at 500 ppm was 41.9 when the sensor was heat to 275 °C. Wu et al. [10] fabricated based V_2O_5 hollow sphere film sensor, which showed a response of 9.7–500 ppm of TEA at 370 °C. Sui et al. [11] synthesized flower-like hierarchical structures of α-MoO_3, and the response to 100 ppm of TEA attained 416 at 250 °C. Yang et al. [17] obtained the optimal TEA sensing properties of TiO_2 nanorod array at an operating temperature of 290 °C. Wang et al. [18] prepared SnO_2 nanorods to detect TEA with a response of 3–1 ppm TEA at 350 °C. Liu et al. [19] synthesized three-dimensional (3D) porous ZnO foam to detect TEA at working temperature as high as 350 °C, and the response was 12–10 ppm TEA. In general, TEA gas sensors can work effectively

* Corresponding author.
E-mail addresses: mse_caobq@ujn.edu.cn, caobingqiang@foxmail.com (B. Cao).

http://dx.doi.org/10.1016/j.snb.2017.01.136
0925-4005/

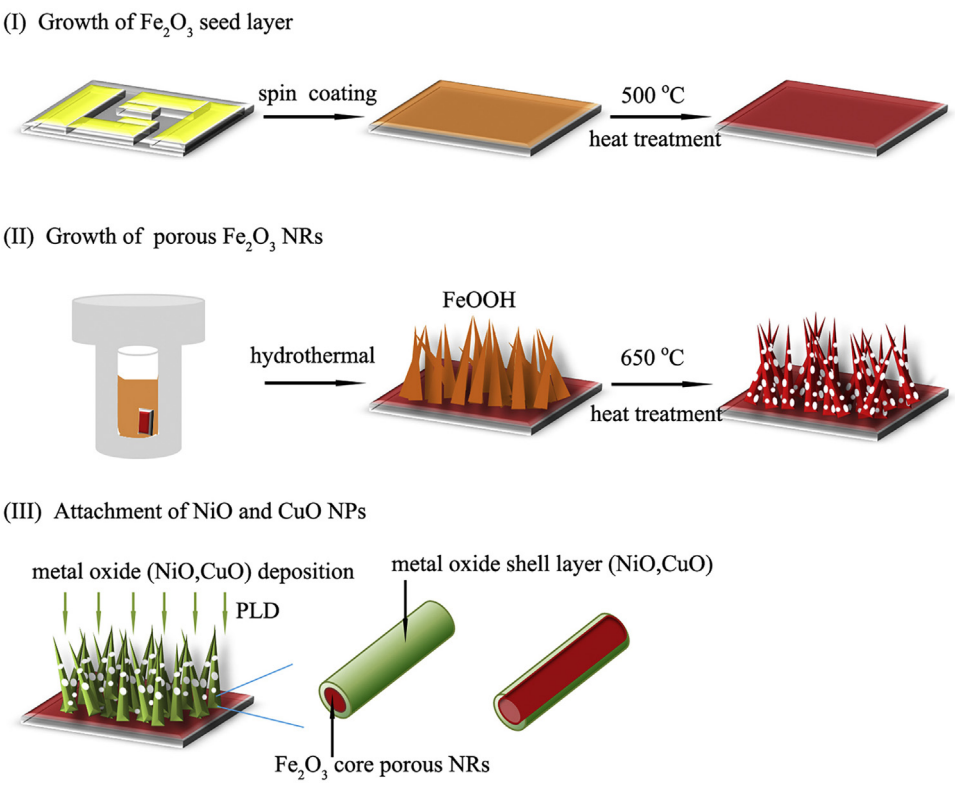

Fig. 1. Schematic illustration for the in-situ growth process of α-Fe_2O_3@NiO/CuO core–shell NRs.

only at high temperature of 300–400 °C [20]. This can result in high energy consumption and fast device degradation due to the agglomeration of small metal oxide particles [7]. Therefore, it is still a challenge to design chemiresistive sensors with low working temperature and high response. Some strategies have been adopted to overcome those shortcomings and building one-dimensional (1D) core–shell heterojunction at interface is reported to be one of the effective ways to improve gas sensing properties [15,21]. For instance, core–shell α-Fe_2O_3@NiO nanofibers exhibited higher response (12.8) to 50 ppm HCHO and faster response/recovery time (2–9 s) than pristine NiO and α-Fe_2O_3 nanofibers [15]. The ZnO-particles decorating α-Fe_2O_3 nanorods exhibited good sensitivity and selectivity to *n*-butanol gas at an optimum temperature of 225 °C [22]. The response of α-Fe_2O_3/SnO_2 core-shell nanorods was up to 19.6 under 10 ppm of ethanol at 220 °C, and the response and recovery times also became shorter [23]. Such improved sensing performance was generally explained by the formation of heterojunctions. But, the basic rule for the fabrication of such heterojunction is still unclear.

According to the proposed sensing mechanism [8,15], the fabrication of such heterojunction needs to be well controlled in terms of many aspects of materials. The intrinsic physical characteristics of semiconductor material such as doping type (n or p type), the work function, and free carrier concentration, are all very important to design the semiconductor heterojunction. Owing to the different position of Fermi energy level (E_F), a depletion layer will form at the heterointerface when two different materials contact each other. In gas-sensing reaction, the electron exchange occurs in a surface layer whose width is the Debye length of sensing material [23]. Recently, Kim et al. [24] proposed that CuO-ZnO core (p)-shell (n) nanowires could significantly enhance the gas sensing properties for reducing gas, particularly, when the shell width was less than its λ_d. Park et al. [25] reported that the In_2O_3-core/ZnO-shell nanowires exhibited the highest response to ethanol when the ZnO shell layer thickness was equivalent to $2\lambda_d$, and the width of the depletion layer was equal to λ_d (In_2O_3)+λ_d (ZnO) due to In_2O_3-ZnO interface. Therefore, the sensing properties of 1D core-shell heterostructure are greatly correlated to the Debye length (λ_d) of the shell material. To enhance the sensing performances of core (n)-shell (p) heterojunction sensor, the Debye length should be taken as a critical parameter for the modulation of shell thickness.

Herein, we successfully fabricate TEA sensors constructed with α-Fe_2O_3@NiO or α-Fe_2O_3@CuO core-shell nanorods and demonstrate that their sensing performance can be greatly improved by optimizing the shell thickness based on the Debye length. Porous α-Fe_2O_3 NRs are grown directly on a flat substrate via a hydrothermal method. NiO and CuO, as typical p-type semiconductors with gas sensing and catalytic properties [15,26], are selected to fabricate core (n)-shell (p) heterojunction sensor by pulsed laser deposition. This method simplifies the traditional gas sensor fabrication process by hand coating. The dependence of the core-shell NRs sensing properties on the p-type shell layer thickness is systematically investigated. Due to the formation of PN heterojunction, the core-shell heterostructural sensors exhibit high response and selectivity at operating temperature as low as 40 °C. It is found that the core-shell sensor with the shell thickness being on the order of λ_d achieves best sensing capabilities and the detailed sensing mechanism is discussed.

2. Experimental section

2.1. Direct growth of porous α-Fe_2O_3 NRs on flat Al_2O_3 electrodes

All reagents were purchased from Sinopharm Chemical Reagent (Shanghai, China) without any refinement. In a typical experiment, hematite seed layer was formed on the cleaned flat Al_2O_3 substrates (1 mm × 1.5 mm) by spin coating (4000 rpm for 30 s) a solution composed of 4.054 g $FeCl_3{\cdot}6H_2O$, 0.211 g polyvinyl alcohol (PVA), 150 μL HCl (36.5–38%), and 50 mL deionized (DI) water, followed by annealing at 500 °C in air for 2 h. 0.810 g $FeCl_3{\cdot}6H_2O$

and 2.548 g $NaNO_3$ were dissolved in 30 mL DI water under stirring constantly to get a yellow aqueous solution. Then 90 μL HCl and 160 μL acetonitrile were added to the above solution. This solution was transferred to a 50 mL Teflon-lined autoclave, and the substrates with seed layer were immersed into the solution, which was then placed within an oven maintained at 100 °C for 4 h. Finally, the precursors were annealed in air at 650 °C for 20 min to obtain the porous α-Fe_2O_3 NRs.

2.2. Growth of α-Fe_2O_3@NiO and α-Fe_2O_3@CuO core–shell NRs

The surface of α-Fe_2O_3 NRs was decorated with a shell layer by PLD at room temperature using NiO or CuO target. A KrF laser of 260 mJ/cm^2 and a vacuum pressure of 0.1 Pa were typically adopted. By changing the laser pulses of 500, 1000, and 1500, α-Fe_2O_3@NiO or α-Fe_2O_3@CuO core–shell NR heterostructures with different shell thickness were grown on flat Al_2O_3 substrates. The schematic process for the growth procedure of core–shell NRs is shown in Fig. 1. The core-shell heterostructures may have two forms, e.g. α-Fe_2O_3 NRs partially or fully covered by p-type NiO or CuO shell.

2.3. Materials characterization and sensing measurement

The morphology and microstructure of as-prepared samples were measured using field emission scanning electron microscope (FESEM, FEI QUANTA FEG250) with energy dispersive X-ray spectroscopy (EDS, INCA MAX-50) and high-resolution transmission electron microscope (HRTEM, JEM-2100F, JEOL). The phase of sensing materials was investigated by X-ray diffraction (XRD, D8-Advance, Bruker) and X-ray photoelectron spectroscopy (XPS, Thermo ESCALAB 250XI). The Brunauer-Emmett-Teller (BET) specific surface areas of the samples were examined through measuring nitrogen adsorption–desorption isotherm (Micromeritics Instrument Corporation TriStar II 3020). The gas-sensing properties of the α-Fe_2O_3 NRs and the core-shell NRs sensors were measured by WS-60A gas-sensing test system (Weisheng, China). The detailed measuring procedures and testing gases conversion formula were reported in our previous work [3]. The sensor response (R) was calculated by $R = R_a/R_g$, where R_a and R_g were the resistances of the sensors in air and in target gas, respectively. The response and recovery times (T_{res} and T_{rec}) of a gas sensor are usually defined as the time required for the resistance to reach 90% of its steady-state value after introduction or removal of the target gas, respectively [7].

3. Result and disscution

3.1. Structure and morphology characterization of core/shell nanorods

XRD was measured to analyze the composition and crystalline phases of the final samples. The peaks in spectrum I of Fig. 2 match well with PDF card (JCPDS No. 75-1594), indicating FeOOH NRs on flat Al_2O_3 substrate are obtained. After annealing at 650 °C for 20 min, pure hematite (α-Fe_2O_3) is observed in spectrum II (JCPDS No. 89-0597). The dehydration and dehydroxylation reactions of FeOOH NRs during the calcinations procedure result in the growth of porous α-Fe_2O_3 NRs [21], as shown as the inset of Fig. 3(a). When NiO and CuO nanoparticles were deposited onto α-Fe_2O_3 NRs, the peaks of NiO and CuO cannot be observed in spectrum III and IV, owing to their low deposition content.

The microstructures of α-Fe_2O_3 and the core-shell NRs were then investigated. Fig. 3(a) shows the α-Fe_2O_3 NRs in-situ grown on the substrate with a seed layer. The inset of Fig. 3(a) reveals their diameters are roughly about 120 nm and numerous micropores are also observed in the NRs. Porous materials possessing lager accessible surface area can greatly accelerate the test gas diffusion and improve the gas sensing performances [27,28]. Fig. 3(b) is the corresponding EDS spectrum of α-Fe_2O_3 NRs. The peaks of O, Fe, and Al can be clearly seen in this spectrum. No other impurities peaks exist, demonstrating again the growth of pure α-Fe_2O_3 NRs on flat Al_2O_3 substrates. Fig. 3(c–h) are SEM images and corresponding EDS spectra of α-Fe_2O_3@NiO core–shell NRs grown with 500, 1000, and 1500 laser pulses, respectively, illustrating that the NRs array morphology can be well maintained after the NiO shell decorating on the α-Fe_2O_3 NRs. In addition to the Fe, O, and Al peaks, the EDS spectra of the α-Fe_2O_3@NiO NRs clearly show the presence of Ni element. The Ni content increases with the increasing of applied laser pulses, which indicates the increase in the thickness of NiO shell, as shown in the insets of Fig. 3(c, e and g). The SEM images of α-Fe_2O_3@CuO core–shell NRs and their corresponding EDS spectra are shown in Fig. S1, which exhibits similar results as Fig. 3.

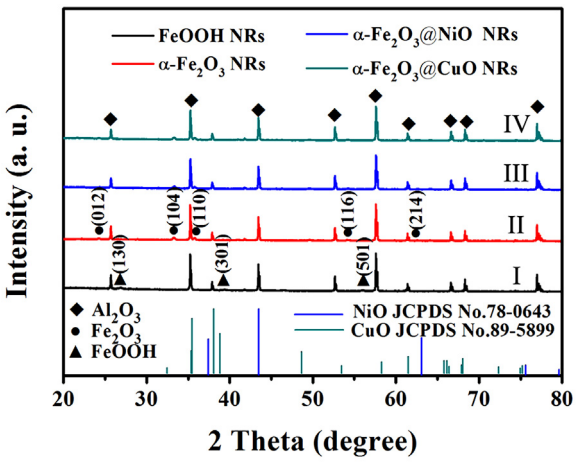

Fig. 2. XRD spectra of as-synthesized: (I) FeOOH; (II) α-Fe_2O_3; (III) α-Fe_2O_3@NiO; (IV) α-Fe_2O_3@CuO NRs grown on flat Al_2O_3 substrate.

To gain further insight into the microstructure and crystallographic feature of the α-Fe_2O_3, α-Fe_2O_3@NiO, and α-Fe_2O_3@CuO NRs, TEM characterizations were performed. The TEM image of Fig. 4(a) shows the α-Fe_2O_3 NRs with porous structure, which is good agreement with the SEM result. The typical length of the NR is about 1 μm and the diameter is about 120 nm. Fig. 4(b) depicts the fringe spacings of 0.220 nm and 0.271 nm corresponding to the (113) and (104) planes of α-Fe_2O_3, respectively. The TEM images of the α-Fe_2O_3@NiO NRs grown with different number of laser pulses are shown in Fig. 4(c–e). Two different shapes of the core-shell heterostructures are observed including p-type shell partially or completely covers α-Fe_2O_3 NRs. This verifies the schematic illustration of the growth process as shown in Fig. 1. The thickness of NiO shells with 500, 1000, and 1500 laser pulses are nearly 6.7 nm, 13 nm, and 18.9 nm, respectively, which is proportional to the number of laser pulses. The lattice spacing of 0.148 nm corresponding to the (220) planes of NiO is also identified as shown in Fig. 4(f), indicating a clear core-shell heterostructure. Fig. 4(g–i) shows that α-Fe_2O_3@CuO NRs grown under different laser pluses (500, 1000, and 1500), and the shell thicknesses are roughly 6.2 nm, 12.4 nm, and 17.9 nm, respectively. Fig. 4(j) reveals the (110), (214), and (012) lattice planes of α-Fe_2O_3. The spacings of 0.231 and 0.252 nm are assigned to (100) and (−111) lattice planes of CuO, indicating the existence of CuO shell layer. Moreover, it is demonstrated that an expected P-N heterointerface is formed between p-type CuO shell and n-type α-Fe_2O_3 NR core.

In order to further characterize the surface composition of the as-synthesized α-Fe_2O_3@NiO and α-Fe_2O_3@CuO NRs, XPS analysis

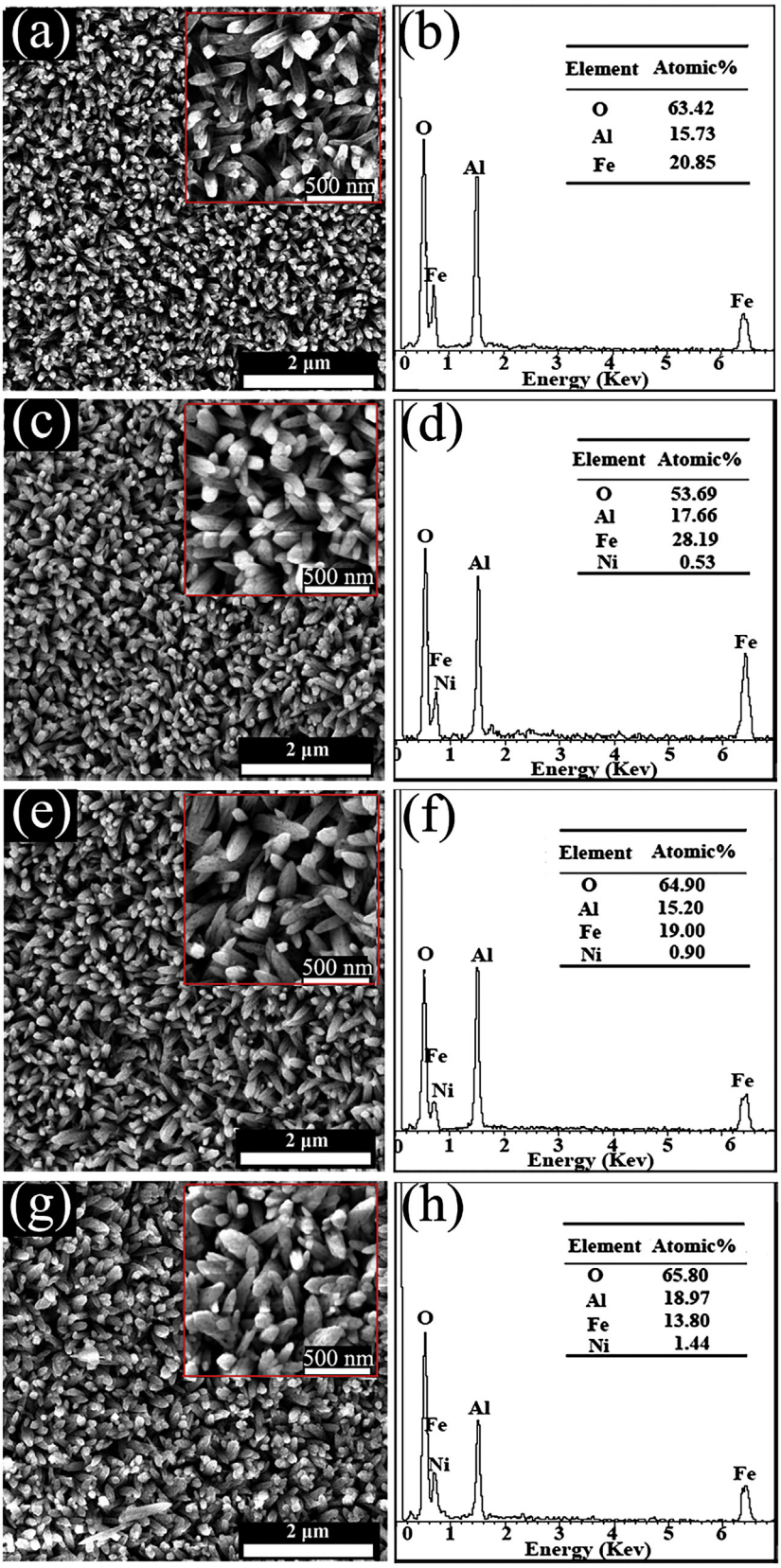

Fig. 3. SEM image and corresponding EDS spectrum of sample directly grown on flat Al_2O_3 substrate: (a and b) porous α-Fe_2O_3 NRs; (c and d) 500-α-Fe_2O_3@NiO core–shell NRs; (e, f) 1000-α-Fe_2O_3@NiO core–shell NRs; (g and h) 1500-α-Fe_2O_3@NiO core–shell NRs. The insets of a, c, e, and g show the enlarged SEM images of the corresponding samples, respectively.

was performed as shown in Fig. 5. Fig. 5(a) reveals the existence of C, O, Fe, and Ni elements, suggesting that the surface of α-Fe_2O_3 NRs is successfully decorated with nickel oxides. Moreover, with the energy difference between Ni $2p_{3/2}$ and Ni $2p_{1/2}$ splitting (18.4 eV), major peaks of Ni $2p_{1/2}$ (872.8 eV) and Ni $2p_{3/2}$ (854.4 eV) confirm the presence of Ni^{2+} from NiO [29]. The shoulder peak at 852.7 eV may be assigned to the Ni^{2+} species on the surface [30]. Fig. 5(d) exhibits four elements (Fe, O, Cu, and C) in the α-Fe_2O_3@CuO NRs arrays. The two peaks of Cu $2p_{3/2}$ and Cu $2p_{1/2}$ locate at 932.2 and 952.0 eV, respectively. The spin-energy separation of the two peaks is 19.8 eV (Fig. 5(f)), indicating the existence of CuO [31,32]. In addition to two satellite peaks at about 715.0 and 729.0 eV, two main peaks center at around 709.4 eV for Fe $2p_{3/2}$ and 723.0 eV for Fe $2p_{1/2}$ as shown in Fig. 5(b) and (e) are all in agreement with the reported peaks for α-Fe_2O_3 [33]. It can be confirmed again that p-type shell are well formed on the surface of the α-Fe_2O_3 NRs arrays by XPS and TEM analysis.

3.2. Improved gas-sensing properties of α-Fe_2O_3@ NiO (CuO) NRs sensor

Fig. S2 in Supporting information (SI) exhibits the images of flat Al_2O_3 substrate with α-Fe_2O_3 NRs and α-Fe_2O_3 NRs gas sensor. The substrate is consisted with a pair of Au electrodes, Pt lead wires, and a heater. As specific surface area is one of important physical parameters for sensing materials, we first compare the sensor properties of commercial Fe_2O_3 powders and the porous nanorods. N_2 adsorption–desorption isotherms (Fig. S3 in SI) are used to calculate the Brunauer-Emmett-Teller (BET) specific surface areas of commercial Fe_2O_3 and porous α-Fe_2O_3 NRs and their BET surface areas are determined to be 13.7 and 22.1 m^2/g, respectively. The responses of commercial Fe_2O_3 and porous α-Fe_2O_3 NRs sensors to 50 ppm TEA at 40 °C are shown in Fig. S3(d). The response of porous α-Fe_2O_3 NRs (R = 8.2) is about 3 times higher than that of commercial Fe_2O_3 (R = 2.6). It reveals that the gas-sensing properties of porous α-Fe_2O_3 NRs are enhanced due to the unique 1D porous nanorod structure, which has good influence on gas diffusion and mass transport [20]. Then the N_2 adsorption–desorption isotherm of α-Fe_2O_3@NiO NRs is also measured, as shown in Fig. S3(c). The BET surface area of α-Fe_2O_3@NiO NRs is 19.7 m^2/g, which is smaller than the pristine α-Fe_2O_3 due to the NiO shell deposition. This means the improved sensor properties (see below) of α-Fe_2O_3@NiO NRs is not due to specific surface area.

As an important parameter, the operating temperature has a great influence on MOS sensor. Fig. 6(a) shows the response curves of the three sensors toward 50 ppm of TEA at different working temperature. The responses of core-shell sensors increase quickly with increasing temperature to 120 °C and then decrease along with increasing temperature. Obviously, the responses of α-Fe_2O_3@NiO and α-Fe_2O_3@CuO sensors reach the maximum values of 24.7 and 27.4, respectively. Such behavior can also be observed in the case of the sensor based on pristine α-Fe_2O_3 NRs. Its maximum response appears at 160 °C, and the value (R = 17) is lower than those of core-shell sensors. The low optimum operating temperature (120 °C and 160 °C) is attributed to the nanoscale porous structure of such sensing materials. In addition, the optimum temperature is also related to the semiconductor heterojunction and detected gas molecules [23]. Owing to the low C—N bond energy (307 kJ/mol), TEA molecules can participate in the gas sensing reaction at relative low temperature [3]. When the sensors work at 40 °C with a heater voltage of 1.18 V, their response to 50 ppm of TEA can maintain at 8.1, 12.2, and 12.9, respectively. The sensor operating at near room temperature can meet with the demand of low power consumption [34]. Hence, the following gas sensing tests were all completed at near room temperature (40 °C).

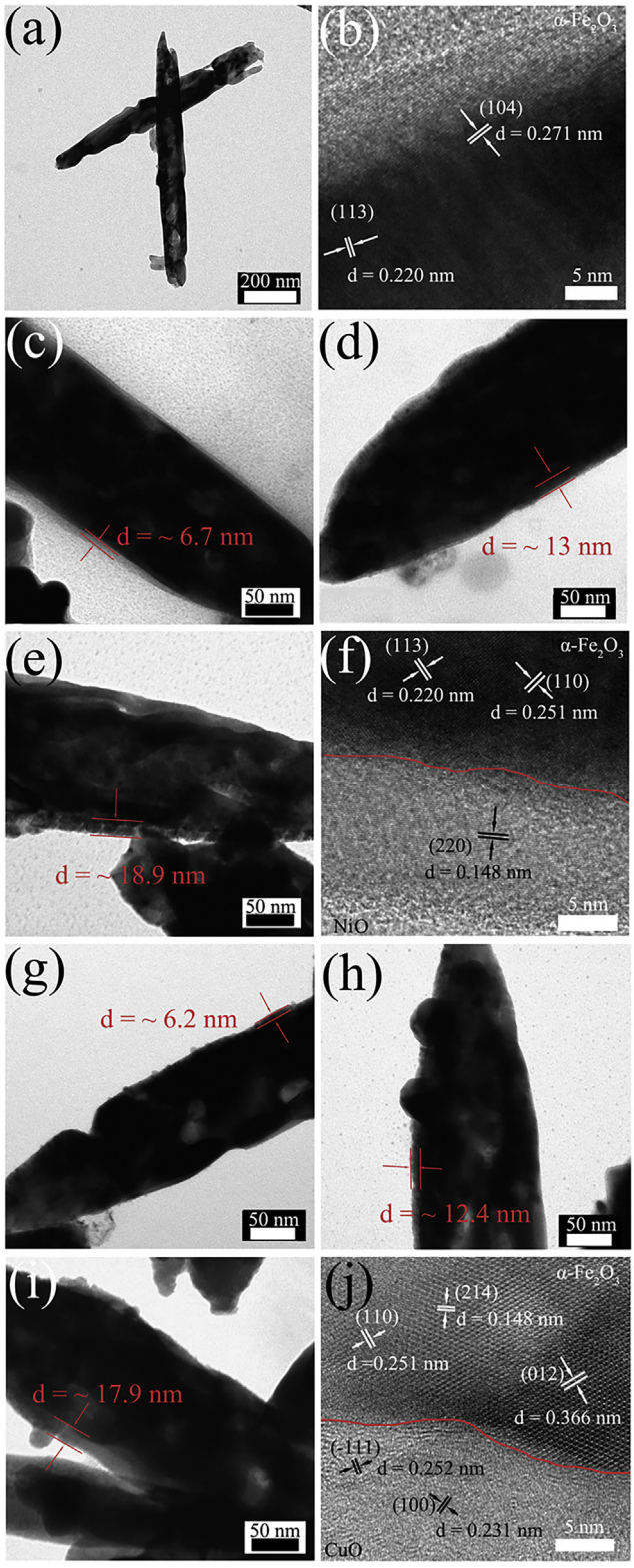

Fig. 4. (a and b) TEM and HRTEM images of porous α-Fe_2O_3; (c–e) TEM images of 500, 1000, and 1500-α-Fe_2O_3@NiO core–shell NRs; (f) HRTEM image of 1000-α-Fe_2O_3@NiO core–shell NRs; (g–i) TEM images of 500, 1000, and 1500-α-Fe_2O_3@CuO core–shell NRs; (f) HRTEM image of 1000-α-Fe_2O_3@CuO core–shell NRs.

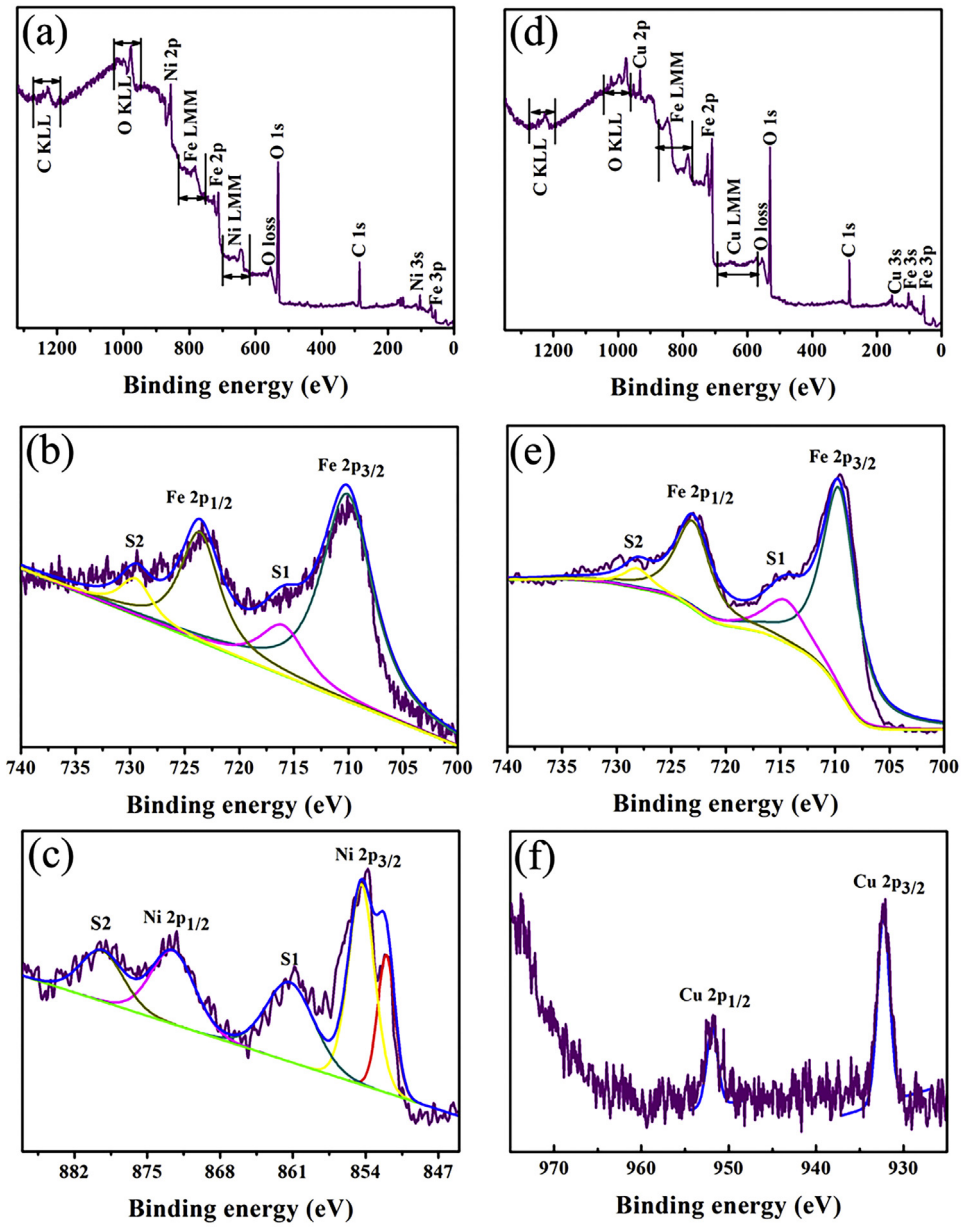

Fig. 5. XPS spectra of α-Fe_2O_3@NiO core–shell NRs: (a) full spectrum; (b) Fe 2p; (c) Ni 2p. XPS spectra of α-Fe_2O_3@CuO core–shell NRs: (d) full spectrum; (e) Fe 2p; (f) Cu 2p.

The relative humidity (RH) is a significant condition for sensor applications. So we also measured the relationship of sensor response and relative humidity at 40 °C, as illustrated in Fig. 6(b). The responses of all sensors decrease with an increase in RH, and a variety of reasons have been discussed [35–38]. First, water vapor can absorb electron from oxygen molecule or analytic gas molecule, which leads to the decrease of R_a and increase of R_g [35,36]. Second, water molecules are preferentially absorbed at the sensing material interface, competing with TEA for the same sites [37]. In addition, OH-groups from water vapor can act as acceptors and react with TEA gas [38]. However, when the RH reaches 50%, the responses of core-shell heterostructure sensors are still higher than that of pure α-Fe_2O_3 NRs sensor.

The obtained response and recovery characteristic curves against TEA of different concentrations (1–50 ppm) for the three sensors are shown in Fig. 7(a). The responses of all sensors increase with the increasing TEA concentration. The α-Fe_2O_3@NiO and α-Fe_2O_3@CuO NRs sensors always exhibit higher response values than pristine α-Fe_2O_3 NRs sensor under the same test concentration. Fig. 7(b) compares their sensitivity as a function of TEA concentration at 40 °C. The core-shell NRs sensors show approximately 2 times higher response than pristine α-Fe_2O_3 sensor. These results clearly reveal that the formation of PN heterojunction is beneficial to improving gas sensing property. Fig. 7(c) shows a typical reproducible run of the core-shell heterostructure sensors after five cycles to 50 ppm of TEA at 40 °C, illustrating that the sensors have good reproducibility.

The response and recovery time in Fig. 8, a significance parameter for estimating gas sensor performance, were also measured. The response time of pure α-Fe_2O_3 NRs sensor is 7 s, which is faster than those (8 s) of core-shell sensors. But all of three sensors take a long time (~20 s) to recover its initial resistance state. Chemiresistive gas sensor working at 40 °C is irreversible due to the fact that the thermal energy is generally lower than the activation energy for desorption [39].

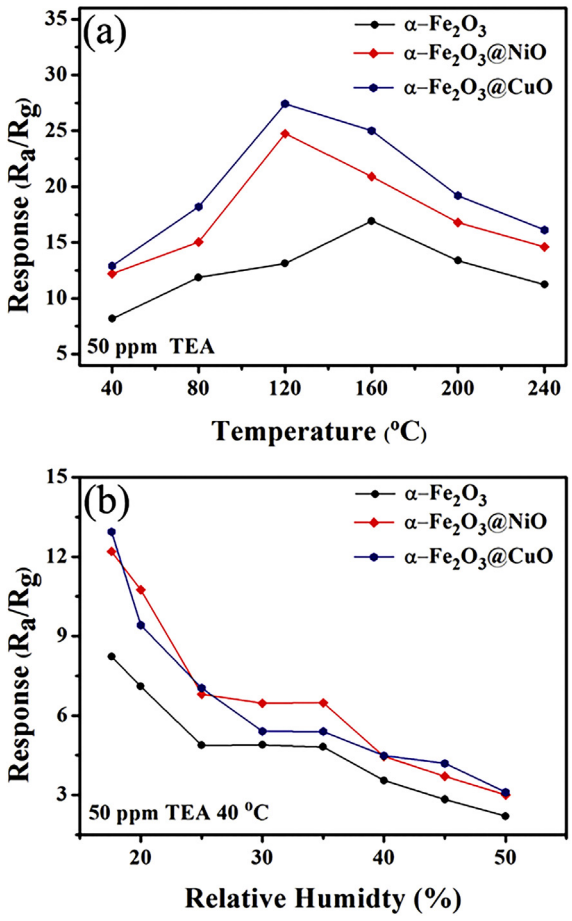

Fig. 6. (a) Responses of α-Fe_2O_3, 1000-α-Fe_2O_3@NiO, and 1000-α-Fe_2O_3@CuO NRs sensors to 50 ppm of TEA at different working temperature with 16% RH; (b) The relationship between the sensor response and relative humidity.

Fig. 9(a) exhibits the responses of three sensors to 50 ppm of various testing gases at 40 °C. The testing gases include triethylamine, acetone, ethanol, benzene, *p*-xylene, and 2-propanol. Obviously, all the sensors to TEA show the highest response compared with those of other gases. The response values of the core-shell sensors to TEA are about 12–13, which are 2–3 times higher than those of other gases, indicating a high selectivity for TEA gas. Improved selectivity of the core-shell sensors toward TEA at near room temperature is observed, while the detailed reason is still unclear for us. One possible reason is the different reaction activity according to bond energy of target gases. For instance, the bond energy of C—N (TEA), C—C (2-propanol), O—H (ethanol), C=C (benzene), and C=O (acetone), is 307, 345, 458.8, 610.3, and 798.9 kJ/mol, respectively [3,7]. Owing to the low C—N bond energy, the high reaction activity of TEA molecules is conducive to the improved selectivity. The long-term stability of three sensors over 50 days were also measured as depicted in Fig. 9(b). The responses of three sensors show almost constant value to 50 ppm of TEA at 40 °C, demonstrating the high stability of these gas sensors.

3.3. Optimizing the sensor response based on debye length

The sensing gas mechanism of α-Fe_2O_3 NR sensor can be explained via the space-charge or depletion layer model [20]. It is depended on the change of surface resistance caused by the adsorption and desorption of the target gas molecules. For this gas sensing mechanism, the thickness of the surface depletion layer is known

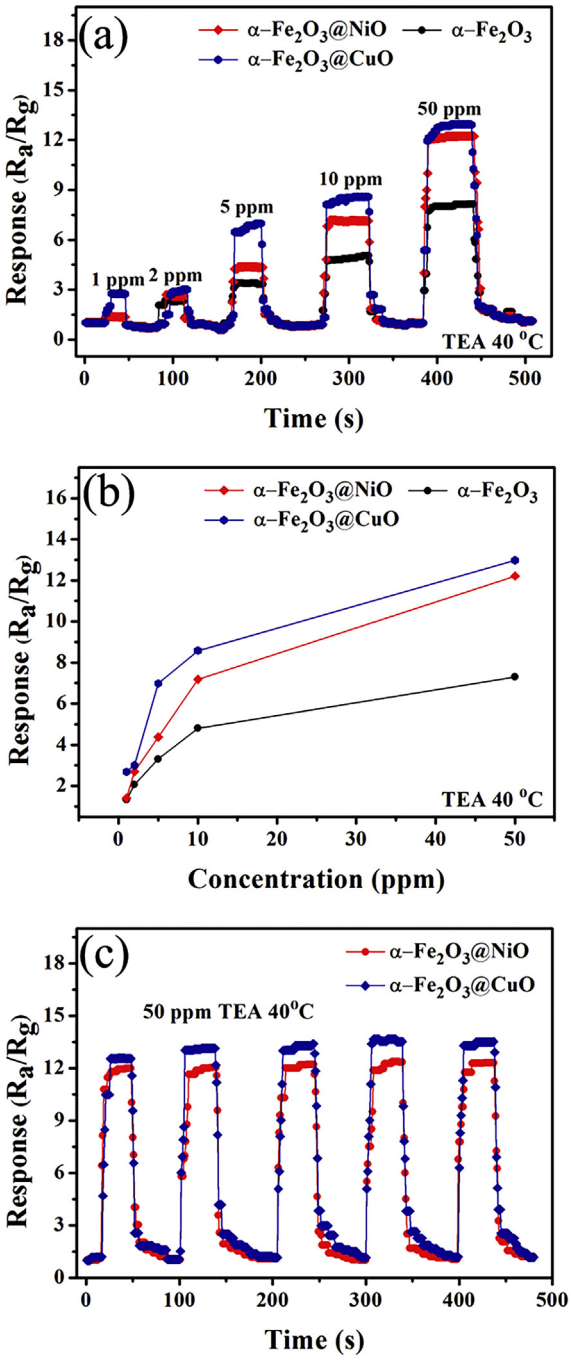

Fig. 7. (a) Response comparison of the three sensors (α-Fe_2O_3, 1000-α-Fe_2O_3@NiO, and 1000-α-Fe_2O_3@CuO NRs) to TEA in the detection range of 1–50 ppm at 40 °C; (b) Corresponding relationship between sensor response and TEA concentration; (c) Repeatability test of the two kinds of sensors to 50 ppm of TEA at 40 °C.

to be on the order of Debye length of the sensing material [23]. λ_d is estimated as follows [40]:

$$\lambda_d = \left(\varepsilon KT/q^2 N_c\right)^{1/2} \quad (1)$$

where ε is the static permittivity, k is the Boltzmann constant (=1.38 × 10^{-23} J/K), T is the absolute temperature (=313 K), q is the electrical charge of an electron (=1.6 × 10^{-19} C), and N_c is the free carrier concentration. As shown in Fig. 10(a), an electron depletion layer will form on the surface of pure α-Fe_2O_3 NR, due to the chemical adsorption of oxygen molecules which extract electrons to become oxygen ions ($O^{\delta-}$). The electron depletion layer

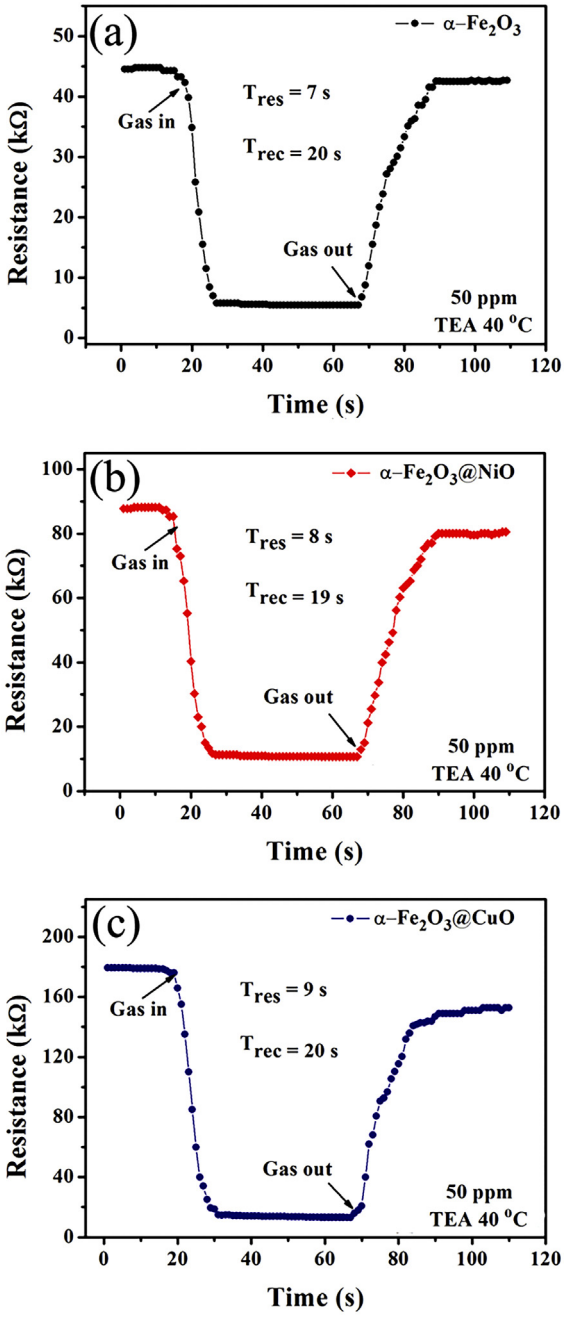

Fig. 8. Response and recovery time of three sensors: (a) α-Fe_2O_3 NRs sensor; (b) 1000-α-Fe_2O_3@NiO NRs sensor; (c) 1000-α-Fe_2O_3@CuO NRs sensor.

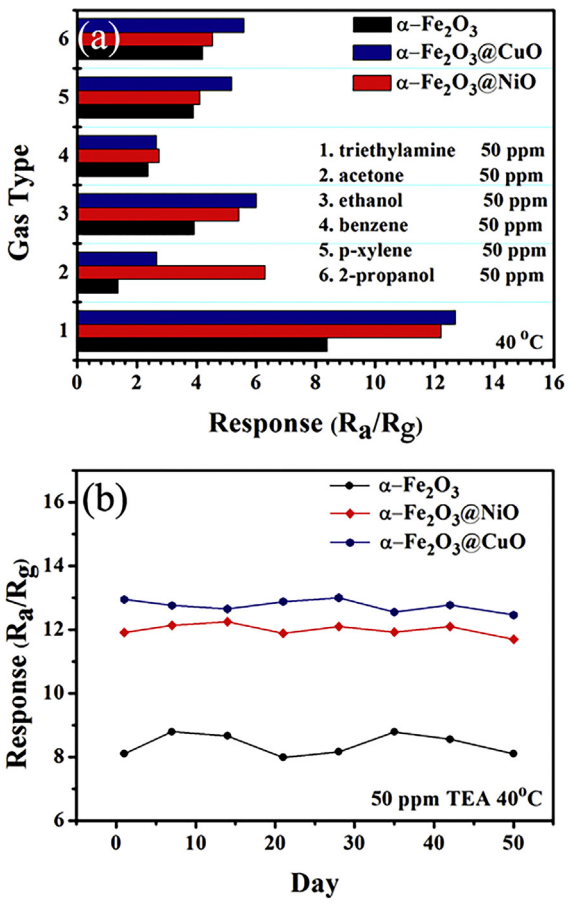

Fig. 9. (a) The selectivity comparison of three sensors for different target gases at 40 °C; (b) Long-term stability of the three sensors to 50 ppm of TEA at 40 °C.

thickness is λ_d (12.3 nm) of α-Fe_2O_3 [41,42]. The potential barrier increases with an increasing number of $O^{\delta-}$ ions on the surface, resulting in a higher resistance state (R_a) [25]. The adsorbed $O^{\delta-}$ will disappear from the α-Fe_2O_3 surface when the TEA gas is supplied, because TEA molecules can react with them and produce N_2, CO_2, and H_2O. Meanwhile, the captured electrons are released back into the conduction band of α-Fe_2O_3, suppressing the depletion layer and decreasing the potential barrier. Consequently, the resistance of pure α-Fe_2O_3 decreases, leading to a lower resistance state (R_g). So, the change in depletion layer of material is a direct factor that influences the gas sensing properties. However, in our experiment, the α-Fe_2O_3 nanorod core has a diameter of about 50–100 nm, which is much larger than the Debye length. The electrons of pristine α-Fe_2O_3 nanorod cannot be completely depleted to participate in gas sensing reaction. To further improve the gas sensing performances, the composite sensors with core-shell PN heterostructure were fabricated by PLD method.

Although NiO or CuO as catalysts can promote selective oxidation of various volatile organic compounds or adsorbed oxygen [26,43], the above enhanced sensing performance of α-Fe_2O_3@NiO and α-Fe_2O_3@CuO composites is mainly due to the formation of PN heterojunction [44]. And the mechanism has been explained via the additional PN depletion layer model in previous works [3,45,46]. Because the Fermi level of n-type semiconductor (α-Fe_2O_3) is higher than p-type semiconductor (NiO or CuO), the electrons will flow from α-Fe_2O_3 to p-type semiconductor, while the holes will flow along the opposite direction of the electrons until their Fermi levels equilibrate [40,44]. This induces the formation of PN heterojunction and an additional depletion layer at the interface. Therefore, the resistance of PN heterostructure in air (R_a) will be even higher than pure α-Fe_2O_3 semiconductor (without the PN heterojunction) due to the expansion of depletion layer at the PN junction interface [45]. Based on the definition of response ($R = R_a/R_g$), the response to the reducing gas is greatly improved by the variation of resistance in air due to the formation of PN heterojunction. So, the radial modulation of the depletion layer caused by the increase of resistance in a PN heterostructure is critical to gas sensing performance [24,25,47].

To further investigate the radial modulation of depletion layer, the influence of the shell thickness on the gas sensing response was optimized. Fig. 11(a) and (b) show the corresponding resistance curves of α-Fe_2O_3, α-Fe_2O_3@NiO, and α-Fe_2O_3@CuO nanorod sensors for 50 ppm TEA at 40 °C. The initial resistances of α-Fe_2O_3

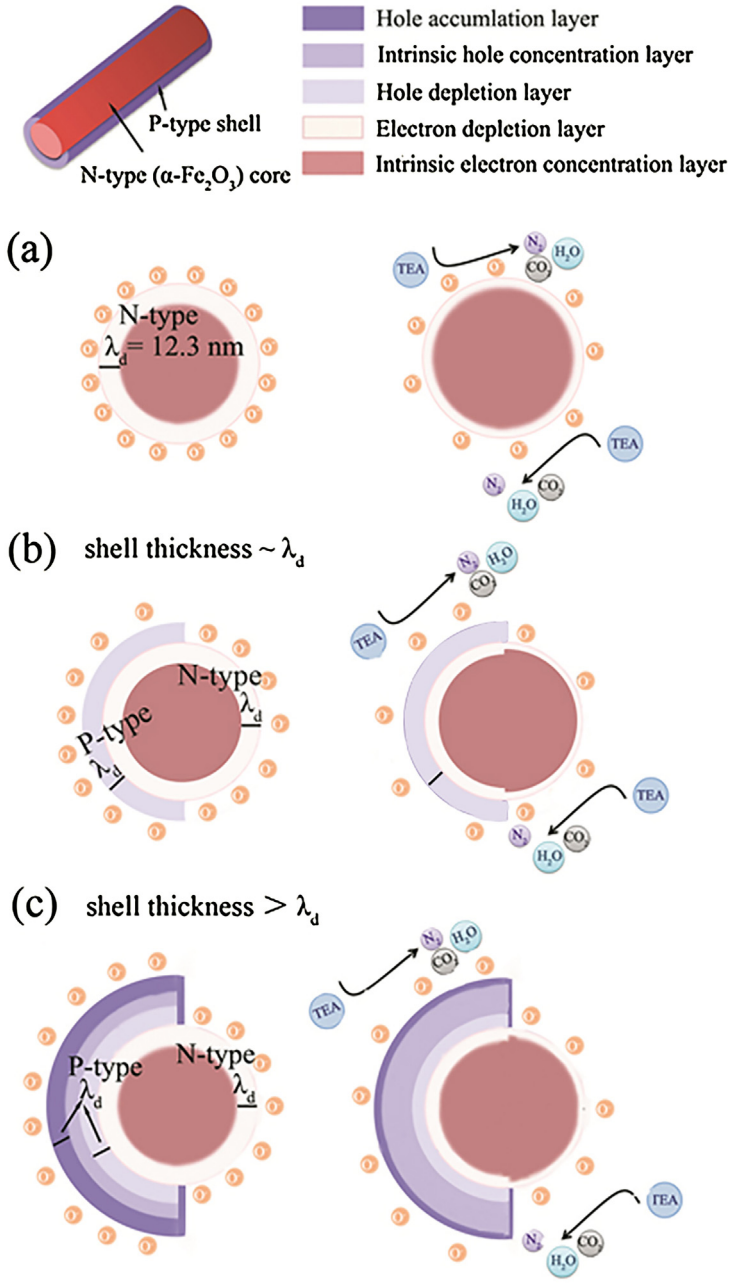

Fig. 10. Schematic of the TEA gas sensing mechanism: (a) Pure α-Fe_2O_3 NRs; (b) Core-shell heterostructure with p-type shell thickness ~ λ_d; (c) Core-shell heterostructure with p-type shell thickness > λ_d.

NRs with p-type shells are much higher than pure α-Fe_2O_3 NRs owing to the formation of a PN depletion region in the core-shell NR. The resistances of all sensors decrease upon exposure to TEA gas and increase during the process of gas desorption. This behavior is typical for an n-type semiconductor sensor, indicating that the p-type shell layer only partially cover the α-Fe_2O_3 NR core, which is consistent with the TEM results. The n-type material of core-shell heterostructures sensor still dominates the sensing performances. Moreover, the recovery resistance is lower than the initial one because the porous nanostructures may still contain some residual TEA gas, which will occupy the absorbing positions of oxygen [48]. Fig. 11(c) summaries the responses of the sensors when the shell thickness is different, which it is controlled by the applied PLD laser pulses. As we can see, the responses of α-Fe_2O_3@NiO sensors increase quickly with increasing shell thickness to 13 nm and then decrease along with increasing thickness. Such a trend can also be observed from α-Fe_2O_3@CuO NRs sensor. The highest response of α-Fe_2O_3@CuO is notably obtained for the shell layer with a thickness of 12.4 nm. Except the α-Fe_2O_3@CuO NRs grown with 1500 laser pulses, all the core-shell NR heterostructures exhibit higher response than pure α-Fe_2O_3 NRs. When the thickness of p-type CuO shell is too thick such as α-Fe_2O_3@CuO NR (1500) sensor, the shell layer may limit the exposure of α-Fe_2O_3 NR to gas and its hole cannot be completely depleted to participate in gas sensitive reaction [25]. This will depress the sensor properties to reducing gas like TEA. It manifests that PN heterojunction only improves the gas-sensing performances under a suitable p-type shell thickness. Furthermore, optimizing the shell thickness in this range is the key for improving sensor response.

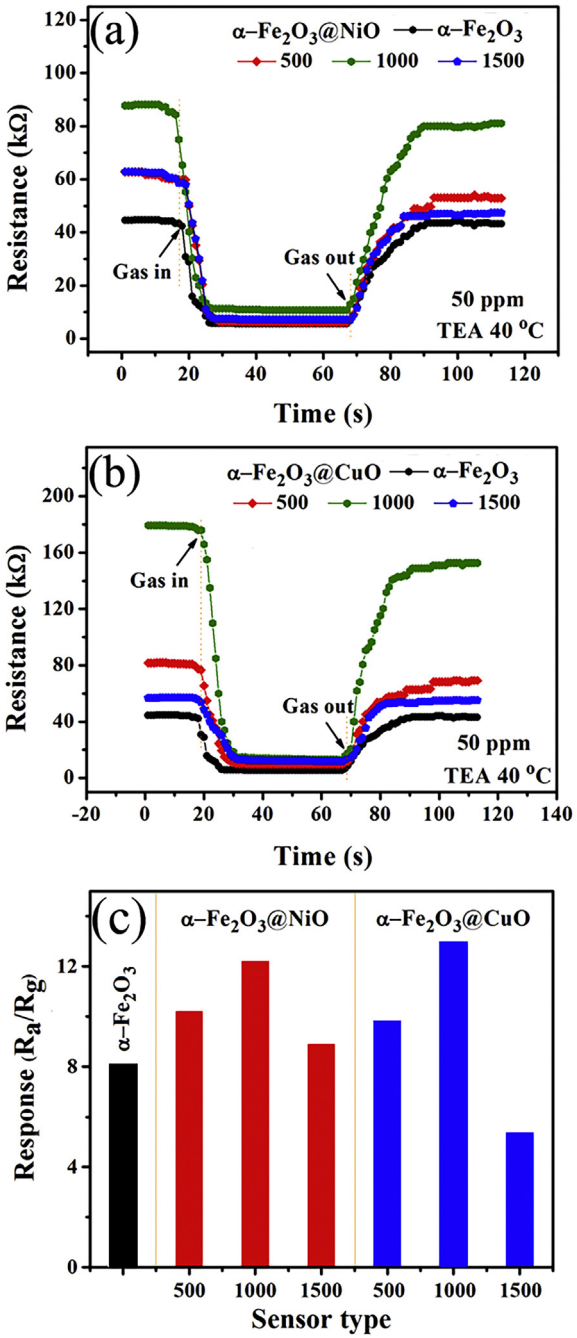

Fig. 11. (a) Resistance curves of α-Fe_2O_3 and α-Fe_2O_3@NiO NR with various shell thickness to 50 ppm of TEA at 40 °C; (b) Resistance curves of α-Fe_2O_3 and α-Fe_2O_3@CuO NR with various shell thickness to 50 ppm of TEA at 40 °C; (c) The response of seven sensors to 50 ppm of TEA at 40 °C.

The sensing performance in this paper suggests that the highest responses of core-shell NR heterostructures are obtained for the p-type shell with a layer thicknesses of about 13 and 12.4 nm, which are very close to the λ_d of NiO and CuO, respectively [40]. As shown in Fig. 10(b) and (c), the holes in a p-type shell with thickness thinner than λ_d will be completely depleted upon exposure to air, leading to a higher resistance. When the shell thickness increases to λ_d, the depletion layer is supposed to be λ_d (NiO or CuO) + λ_d (α-Fe_2O_3)) [25]. In this case, the value of resistance (R_a) in air can reach the maximum. Once the heterostructure is exposed to TEA gas, the $O^{\delta-}$ adsorbed on the sample surface react with TEA molecules and release the electrons back to the sample, causing the decrease of sensor resistance (R_g). In the case of p-type shell thickness larger than λ_d, the holes in the shell are only partly depleted by the formation of PN heterojunction. Moreover, the shell is also in a state of partial hole-accumulation due to the chemical adsorption of oxygen molecules, which pull out electrons in the bulk to become $O^{\delta-}$. The thicker shell may have a weaker influence on resistance modulation. Based on the fundamental sensor response theory ($R = R_a/R_g$), the enhanced response depending on the bigger initial resistance (R_a) changes is due to the formation of PN heterojunction. Therefore, the best sensing performance of core-shell heterostructure can be achieved by optimizing the p-type shell thickness based on Debye length.

4. Conclusions

In short, we design near room-temperature TEA gas sensor with α-Fe_2O_3@NiO(CuO) core-shell heterostructure NRs and their improved gas sensing mechanism based on the modulation of depletion layer at interface is discussed in detail. The core porous α-Fe_2O_3 NRs directly grow on the flat Al_2O_3 substrates and the p-type shell thickness is controlled by the applied laser pulses. Owing to the formation of PN heterojunction, the core-shell sensors show high response, good repeatability, and excellent selectivity to TEA gas at temperature as low as 40 °C. When the shell thickness is optimized to Debye length (λ_d) of p-type semiconductor shell, the core-shell NRs sensor exhibits the best gas-sensing performance. The improved gas sensing performance of such core-shell heterostructural sensor is attributed to the great change in initial resistance caused by optimizing the p-type shell thickness based on Debye length. This study offers an effective way for fabrication of the chemiresistance gas sensors with high performance.

Acknowledgments

This work is supported by NSFC (51472110) and Shandong Provincial Science Foundation (JQ201214, 2014ZRB019JP). The research programs from Ministry of Education, China, are also acknowledged (213021A). BC thanks the Taishan Scholar Chaired Professorship tenured at University of Jinan.

Appendix A. Supplementary data

Supplementary data associated with this article can be found, in the online version, at http://dx.doi.org/10.1016/j.snb.2017.01.136.

References

[1] L. Xu, H.J. Song, J. Hu, Y. Lv, K.L. Xu, A cataluminescence gas sensor for triethylamine based on nanosized LaF_3–CeO_2, Sens. Actuators B 169 (2012) 261–266.
[2] J.A. Young, Triethylamine, J. Chem. Educ. 84 (2007) 926.
[3] Q. Xu, D.X. Ju, Z.C. Zhang, S. Yuan, J. Zhang, H.Y. Xu, B.Q. Cao, Near room-temperature triethylamine sensor constructed with CuO/ZnO P-N heterostructural nanorods directly on flat electrode, Sens. Actuators B 225 (2016) 16–23.
[4] S. Lind, S. Aßmann, L. Zigan, S. Will, Fluorescence characteristics of the fuel tracers triethylamine and trimethylamine for the investigation of fuel distribution in internal combustion engines, Appl. Opt. 55 (2016) 1551–1558.
[5] P.A. Smitha, C.R.J. Lepage, P.B. Savagec, C.R. Bowerbank, E.D. Lee, M.J. Lukacs, Use of a hand-portable gas chromatograph—toroidal ion trap mass spectrometer for self-chemical ionization identification of degradation products related to *O*-ethyl *S*-(2-diisopropylaminoethyl) methyl phosphonothiolate (VX), Anal. Chim. Acta 690 (2011) 215–220.
[6] M.A. Lqbal, J.E. Szulejko, K.H. Kim, Determination of methylamine, dimethylamine, and trimethylamine in air by high-performance liquid chromatography with derivatization using 9-fluorenylthylchloroformate, Anal. Methods 6 (2014) 5697–5707.
[7] D.X. Ju, H.Y. Xu, Z.W. Qiu, Z.C. Zhang, Q. Xu, J. Zhang, J.Q. Wang, B.Q. Cao, Near room temperature, fast-response, and highly sensitive triethylamine sensor assembled with Au-loaded ZnO/SnO_2 core–shell nanorods on flat alumina substrates, ACS Appl. Mater. Interfaces 7 (2015) 19163–19171.

[8] C.L. Zhu, H.L. Yu, Y. Zhang, T.S. Wang, Q.Y. Ouyang, L.H. Qi, Y.J. Chen, X.Y. Xue, Fe_2O_3/TiO_2 tube-like nanostructures: synthesis, structural transformation and the enhanced sensing properties, ACS Appl. Mater. Interfaces 4 (2012) 665–671.
[9] S. Vallejos, I. Gracia, E. Figueras, C. Cane, Nanoscale heterostructures based on $Fe_2O_3@WO_{3-x}$ nanoneedles and their direct integration into flexible transducing platforms for toluene sensing, ACS Appl. Mater. Interfaces 7 (2015) 18638–18649.
[10] M.Z. Wu, X.F. Zhang, S. Gao, X.L. Cheng, Z.M. Rong, Y.M. Xu, H. Zhao, L.H. Huo, Construction of monodisperse vanadium pentoxide hollow spheres via a facile route and trimethylamine sensing property, CrystEngComm 15 (2013) 10123–10131.
[11] L.L. Sui, X.X. Song, X.L. Cheng, X.F. Zhang, Y.M. Xu, S. Gao, P. Wang, H. Zhao, L.H. Huo, Ultraselective and ultrasensitive TEA sensor based on α-MoO_3 hierarchical nanostructures and the sensing mechanism, CrystEngComm 17 (2015) 6493–6503.
[12] L.L. Sui, Y.M. Xu, X.F. Zhang, X.L. Cheng, S. Gao, H. Zhao, Z. Cai, L.H. Huo, Construction of three-dimensional flower-like α-MoO_3 with hierarchical structure for highly selective triethylamine sensor, Sens. Actuators B 208 (2015) 406–414.
[13] Z. Lou, F. Li, J. Deng, L.L. Wang, T. Zhang, Branch-like hierarchical heterostructure (α-Fe_2O_3/TiO_2): a novel sensing material for trimethylamine gas sensor, ACS Appl. Mater. Interfaces 5 (2013) 12310–12316.
[14] X. Zhou, C. Wang, W. Feng, P. Sun, X.W. Li, G.Y. Lu, Hollow α-Fe_2O_3 quasi-cubic structures: hydrothermal synthesis and gas sensing properties, Mater. Lett. 120 (2014) 5–8.
[15] J. Cao, Z.Y. Wang, R. Wang, S. Liu, T. Fei, L.J. Wang, T. Zhang, Synthesis of core–shell α-Fe_2O_3 @NiO nanofibers with hollow structures and their enhanced HCHO sensing properties, J. Mater. Chem. A 3 (2015) 5635–5641.
[16] G. Sun, H.L. Chen, Y.W. Li, G.Z. Ma, S.S. Zhang, T.K. Jia, J.L. Cao, X.D. Wang, H. Bala, Z.Y. Zhang, Synthesis and triethylamine sensing properties of mesoporous α-Fe_2O_3 microrods, Mater. Lett. 178 (2016) 213–216.
[17] H.-Y. Yang, X.-L. Cheng, X.-F. Zhang, Z.-K. Zheng, X.-F. Tang, Y.-M. Xu, S. Gao, H. Zhao, L.-H. Huo, A novel sensor for fast detection of triethylamine based on rutile TiO_2 nanorod arrays, Sens. Actuators B 205 (2014) 322–328.
[18] D. Wang, X.F. Chu, M.L. Gong, Gas-sensing properties of sensors based on single-crystalline SnO_2 nanorods prepared by a simple molten-salt method, Sens. Actuators B 117 (2006) 183–187.
[19] J.L. Wang, C.J. Pei, L.J. Cheng, W.P. Wan, Q. Zhao, H.Q. Yang, S.Z. Liu, Responses of three-dimensional porous ZnO foam structures to the trace level of triethylamine and ethanol, Sens. Actuators B 223 (2016) 650–657.
[20] H.J. Song, X.H. Jia, H. Qi, X.F. Yang, H. Tang, C.Y. Min, Flexible morphology-controlled synthesis of monodisperse α-Fe_2O_3 hierarchical hollow microspheres and their gas-sensing properties, J. Mater. Chem. 22 (2012) 3508.
[21] A. Katoch, S.W. Choi, G.J. Sun, S.S. Kim, an Approach to detecting a reducing gas by radial modulation of electron-depleted shells in core–shell nanofibers, J. Mater. Chem. A 1 (2013) 13588–13596.
[22] Y.V. Kaneti, Q.M.D. Zakaria, Z.J. Zhang, C.Y. Chen, J. Yue, M.S. Liu, X.C. Jiang, A.B. Yu, Solvothermal synthesis of ZnO-decoratedα α-Fe_2O_3 nanorods with highly enhanced gas-sensing performance toward N-butanol, J. Mater. Chem. A 2 (2014) 13283–13292.
[23] Y.J. Chen, C.L. Zhu, L.J. Wang, P. Gao, M.S. Cao, X.L. Shi, Synthesis and enhanced ethanol sensing characteristics of α-Fe_2O_3/SnO_2 core–shell nanorods, Nanotechnology 20 (2009) 045502.
[24] J.H. Kim, A. Katoch, S.S. Kim, Optimum shell thickness and underlying sensing mechanism in p–n CuO–ZnO core–shell nanowires, Sens. Actuators B 222 (2016) 249–256.
[25] S. Park, H. Ko, S. Kim, C. Lee, Role of the interfaces in multiple networked one-dimensional core-shell nanostructured gas sensors, ACS Appl. Mater. Interfaces 6 (2014) 9595–9600.
[26] A. Chowdhuri, D. Haridas, K. Sreenivas, V. Gupta, Enhanced oxygen adsorption activity by CuO catalyst cluster on SnO_2 thin film based sensors, in: 3rd International Conference on Sensing Technology Tainan, Taiwan, IEEE, 2008, pp. 553–555.
[27] W.X. Jin, S.Y. Ma, Z.Z. Tie, X.H. Jiang, W.Q. Li, J. Luo, X.L. Xu, T.T. Wang, Hydrothermal synthesis of monodisperse porous cube, cake and spheroid-like α-Fe_2O_3 particles and their high gas-sensing properties, Sens. Actuators B 220 (2015) 243–254.
[28] X.P. Shen, Q. Liu, Z.Y. Ji, G.X. Zhu, H. Zhou, K.M. Chen, Controlled synthesis and gas sensing properties of porous Fe_2O_3/NiO hierarchical nanostructures, CrystEngComm 17 (2015) 5522.
[29] M.A. Peck, M.A. Langell, Comparison of nanoscaled and bulk NiO structural and environmental characteristics by XRD XAFS, and XPS, Chem. Mater. 24 (2012) 4483–4490.
[30] Y.F. Wang, F.D. Qu, J. Liu, Y. Wang, J.R. Zhou, S.P. Ruan, Enhanced H_2S sensing characteristics of CuO–NiO core–shell microspheres sensors, Sens. Actuators B 209 (2015) 515–523.
[31] S. Zhu, M. Wu, M.H. Ge, H. Zhang, S.K. Li, C.H. Li, Design and construction of three-dimensional CuO/polyaniline/rGO ternary hierarchical architectures for high performance supercapacitors, J. Power Sources 306 (2016) 593–601.
[32] S.L. Bai, W.T. Guo, J.H. Sun, J. Li, Y. Tian, A.F. Chen, R.X. Luo, D.Q. Li, Synthesis of SnO_2–CuO heterojunction using electrospinning and application in detecting of CO, Sens. Actuators B 226 (2016) 96–103.
[33] X.F. Lu, X.Y. Chen, W. Zhou, Y.X. Tong, G.R. Li, α-Fe_2O_3@PANI core–shell nanowire arrays as negative electrodes for asymmetric supercapacitors, ACS Appl. Mater. Interfaces 7 (2015) 14843–14850.
[34] D. Miller, S. Akbar, P. Morris, Nanoscale metal oxide-based heterojunctions for gas sensing: a review, Sens. Actuators B 204 (2014) 250–272.
[35] K.I. Choi, H.J. Kim, Y.C. Kang, J.H. Lee, Ultraselective and ultrasensitive detection of H_2S in highly humid atmosphere using CuO-loaded SnO_2 hollow spheres for real-time diagnosis of halitosis, Sens. Actuators B 197 (2014) 371–376.
[36] Z.K. Bai, C.S. Xie, M.L. Hu, S.P. Zhang, D.W. Zeng, Effect of humidity on the gas sensing property of the tetrapod-shaped ZnO nanopowder sensor, Mater. Sci. Eng. B 149 (2008) 12–17.
[37] Z. Ling, C. Leach, The effect of relative humidity on the NO_2 sensitivity of a SnO_2/WO_3 heterojunction gas sensor, Sens. Actuators B 102 (2004) 102–106.
[38] G. Korotcenkov, I. Blinov, V. Brinzari, J.R. Stetter, Effect of air humidity on gas response of SnO_2 thin film ozone sensors, Sens. Actuators B 122 (2007) 519–526.
[39] Z.Y. Fan, J.G. Lu, Gate-refreshable nanowire chemical sensors, Appl. Phys. Lett. 86 (2015) 123510.
[40] F.D. Qu, J. Liu, Y. Wang, S.P. Wen, Y. Chen, X. Li, S.P. Ruan, Hierarchical $Fe_3O_4@Co_3O_4$ core–shell microspheres: preparation and acetone sensing properties, Sens. Actuators B 199 (2014) 346–353.
[41] R.A. Lunt, A.J. Jackson, A. Walsh, Dielectric response of Fe_2O_3 crystals and thin films, Chem. Phys. Lett. 586 (2013) 67–69.
[42] M.C. Huang, W.S. Chang, J.C. Lin, Y.H. Chang, C.C. Wu, Magnetron sputtering process of carbon-doped α-Fe_2O_3 thin films for photoelectrochemical water splitting, J. Alloys Compd. 636 (2015) 176–182.
[43] G.M. Bai, H.X. Dai, J.G. Deng, Y.X. Liu, K.M. Ji, Porous NiO nanoflowers and nanourchins: highly active catalysts for toluene combustion, Catal. Commun. 27 (2012) 148–153.
[44] H.-J. Kim, J.-H. Lee, Highly sensitive and selective gas sensors using p-type oxide semiconductors: overview, Sens. Actuators B 192 (2014) 607–627.
[45] C. Wang, X.Y. Cheng, X. Zhou, P. Sun, X.L. Hu, K. Shimanoe, G.Y. Lu, N. Yamazoe, Hierarchical α-Fe_2O_3/NiO composites with a hollow structure for a gas sensor, ACS Appl. Mater. Interfaces 6 (2014) 12031–12037.
[46] Y.R. Li, C.Y. Wan, C.T. Chang, W.L. Tsai, Y.C. Huang, K.Y. Wang, P.Y. Yang, H.C. Cheng, Thickness effect of NiO on the performance of ultraviolet sensors with p-NiO/n-ZnO nanowire heterojunction structure, Vacuum 118 (2015) 48–54.
[47] H.-J. Kim, H.-M. Jeong, T.-H. Kim, J.-H. Chung, Y.C. Kang, J.-H. Lee, Enhanced ethanol sensing characteristics of In_2O_3-decorated NiO hollow nanostructures via modulation of hole accumulation layers, ACS Appl. Mater. Interfaces 6 (2014) 18197–18204.
[48] S.W. Choi, A. Katoch, J.H. Kim, S.S. Kim, Remarkable improvement of gas-sensing abilities in p-type oxide nanowires by local modification of the hole-accumulation layer, ACS Appl. Mater. Interfaces 7 (2015) 647–652.

Biographies

Qi Xu is a graduate student focusing on heterostructure semiconductor gas sensor working at room temperature for master degree at University of Jinan. She was awarded a B.Sc. degree in materials science and engineering from the same university in 2014.

Zichao Zhang received his BS degree (2013) and MS degree (2016) in Materials Science and Engineering from University of Jinan. His research focuses on the development of nanostructured materials for the application in Li ion batteries.

Xiaopan Song is a graduate student focusing on heterostructure semiconductor gas sensor University of Jinan. She was awarded a B.Sc. degree in materials science and engineering from the same university in 2016.

Shuai Yuan is a graduate student focusing on semiconductor material and device for master degree at University of Jinan. He was awarded a B.Sc. degree in materials science and engineering from the same university in 2014.

Zhiwen Qiu is a Ph.D. Candidate focusing on semiconductor material and device for doctor degree at University of Jinan. She was awarded a master's degree in materials science and engineering from the same university in 2014.

Hongyan Xu is an associate professor at school of materials science and engineering, University of Jinan. Her main research interests are the synthesis and fabrication of semiconductor nanomaterials and conductive polymer composite chemical gas sensors.

Bingqiang Cao is a Taishan Scholar Chair Professor for material physics with University of Jinan. He leads a group focusing on semiconducting oxide thin films, nanostructures, heterostructures, and related devices.